Report
P-21-05
December 2021

Bentonite homogenisation

Three studies based on laboratory test results

Ann Dueck
Lennart Börgesson

SVENSK KÄRNBRÄNSLEHANTERING AB

SWEDISH NUCLEAR FUEL
AND WASTE MANAGEMENT CO

Box 3091, SE-169 03 Solna
Phone +46 8 459 84 00
skb.se

SVENSK KÄRNBRÄNSLEHANTERING

ISSN 1651-4416
SKB P-21-05
ID 1955093

December 2021

Bentonite homogenisation

Three studies based on laboratory test results

Ann Dueck, Lennart Börgesson
Clay Technology AB

Keywords: Bentonite, Swelling, Swelling pressure, Homogenisation.

Abstract

Swelling of the buffer blocks and buffer homogenisation are important functions to guarantee that the requirements of the buffer in a deposition hole and the backfill in the tunnels are fulfilled after full water saturation. It is important to understand and be able to predict the final condition of the buffer and backfill after the swelling and homogenisation, which occurs during the initial saturation and homogenisation of the blocks and pellets and also after possible loss of bentonite caused by for example erosion.

To increase the knowledge of the homogenisation process an SKB project has been running during several years. Based on tests and results from this project, analyses of some specific test results have been made and the results are, in this report, presented as three analyses: 1) Comparison of homogenisation and sealing behaviour of calcium bentonite and sodium bentonite, 2) Comparison of homogenisation and sealing behaviour of bentonite after rapid and slow water uptake, and 3) Comparison of homogenisation of bentonite in long steel tubes after two, four and six years.

In the first study the difference in homogenisation and sealing behaviour between a Ca-bentonite and a Na-bentonite was analysed from laboratory tests results. In general, similar homogenisation behaviour was seen in the two bentonite types.

In the second analysis it was shown that the water uptake rate did not influence the maximum and minimum swelling pressure. However, adding water slowly caused a non-symmetrical behaviour towards the water inlet both in dry density and in swelling pressure. After large swelling it was also seen that density gradients were lower in the test with slow water supply and low initial degree of saturation.

In the third analysis it was shown that the understanding of the homogenisation can be further explained by use of the analytical model used. The friction angle evaluated from the analysis was found to agree with previous results determined with another type of test. However, the main purpose of these tests was to study the influence of time on the homogenisation in long tubes. The results indicated a small reduction in friction angle with time but evaluation of results from still running tests, which will be terminated after additional several years, need to be done in order to confirm.

Sammanfattning

Buffertblockens svällning och homogenisering är viktiga egenskaper för att kunna garantera att kraven på bufferten i ett deponeringshål, och återfyllningen i tunnlarna, uppfylls efter full vattenmättnad. Det är också viktigt att förstå och kunna förutsäga buffertens och återfyllnadens slutliga tillstånd som uppstår under den initiala vattenmättnadsfasen efter svällning och homogenisering av block och pellets, och även efter eventuell förlust av bentonit orsakad av till exempel erosion.

För att öka kunskapen om homogeniseringsprocessen har ett SKB-projekt pågått under flera år. Baserat på tester och resultat från detta projekt har analyser av vissa specifika testresultat gjorts och resultaten presenteras i denna rapport som tre analyser: 1) Jämförelse av homogeniserings- och svällningsegenskaper hos kalciumbentonit och natriumbentonit, 2) Jämförelse av homogeniserings- och svällningsegenskaper hos bentonit efter snabbt och långsamt vattenupptag, och 3) Jämförelse av homogenisering hos bentonit som installerats i långa stålrör och som avslutats efter två, fyra och sex år.

I den första studien analyserades skillnaden i homogeniserings- och svällningsegenskaper mellan en Ca-bentonit och en Na-bentonit utifrån resultat från olika laboratorietester. I allmänhet var homogeniseringsbeteendet likartat för de två bentonittyperna.

I den andra analysen visade resultatet att hastigheten hos vattenupptaget inte påverkade det högsta och lägsta uppmätta svälltrycket. Att tillsätta vatten långsamt orsakade dock ett icke-symmetriskt beteende nära vatteninloppet både beträffande torrdensitet och svälltryck. Efter stor svällning var dessutom densitetsgradienterna lägre i försöket med långsam vattentillförsel och låg initial mättnadsgrad.

Den tredje analysen visade att förståelsen för homogenisering kan ökasgenom den analytiska modell som användes. Friktionsvinkeln som utvärderades från analysen visade överensstämmelse med tidigare resultat som bestämts med en annan försökstyp. Huvudsyftet med de aktuella testerna var dock att studera tidens inverkan på homogeniseringen i långa rör. Resultaten indikerade en liten minskning av friktionsvinkeln med tiden men utvärdering av resultat från återstående försök, som kommer att brytas efter ytterligare ett antal år, behövs för att bekräfta detta.

Contents

1	**Introduction**	7
1.1	Background	7
1.2	Objective	7
1.3	Content of the report	7
2	**Comparison of homogenisation and sealing behaviour of calcium bentonite and sodium bentonite**	9
2.1	General	9
2.2	Material	9
2.3	Homogenisation after axial swelling	9
2.4	Homogenisation after loss of bentonite	14
2.5	Concluding remarks	16
3	**Comparison of homogenisation and sealing behaviour after rapid and slow water uptake**	17
3.1	General	17
3.2	Material	17
3.3	Experiment description	17
3.4	Results and comparison	18
3.5	Concluding remarks	22
4	**Comparison of homogenisation of bentonite in long steel tubes after two, four and six years**	23
4.1	General	23
4.2	Material	23
4.3	Experiment description	23
4.4	Resulting measurements	24
4.5	Analysis – Analytical solution	26
4.6	Concluding remarks	30
5	**Final comments**	31
References		33

1 Introduction

1.1 Background

Swelling of the buffer blocks and buffer homogenisation are important functions to guarantee that the requirements of the buffer in a deposition hole and the backfill in the tunnels are fulfilled after full water saturation. It is important to understand and be able to predict the final condition of the buffer after the swelling and homogenisation, which occur during the initial saturation and homogenisation of the blocks and pellets and also after possible loss of bentonite caused by for example erosion.

To increase the knowledge of the homogenisation process an SKB project was initiated and has been running during more than twelve years. The laboratory part of the project consists of different test types e.g. fundamental swelling tests, measurement of friction between bentonite and other surfaces, homogenisation after loss of bentonite (the self-healing tests) and homogenisation in long tubes. Results have been presented in five status reports (Dueck et al. 2011, 2014, 2016, 2018, 2022).

Analyses of some of the test results from the project were presented by Dueck et al. (2019) where results and findings of the project were compiled. In addition, material models have been developed and verified with some of the laboratory test results from this project and presented by Börgesson et al. (2020).

1.2 Objective

The objective with this report is to present analyses of some specific test results provided within this project. The specific analyses are 1) Comparison of homogenisation and sealing behaviour of calcium bentonite and sodium bentonite, 2) Comparison of homogenisation and sealing behaviour of bentonite after rapid and slow water uptake and 3) Comparison of homogenisation of bentonite in long steel tubes after two, four and six years.

1.3 Content of the report

Tests and test results referred to in this report can be further studied in the status report of the project, referred to above. In Chapter 2, 3 and 4 each analysis is presented together with a general description, a short presentation of the material used and concluding remarks. The chapters are planned to be used as poster presentations with addition of an acknowledgement to SKB and a list of references. That is why each chapter begins with a short presentation of the project. Final comments are given in Chapter 5.

2 Comparison of homogenisation and sealing behaviour of calcium bentonite and sodium bentonite

2.1 General

Presently an SKB project is running where the self-sealing and homogenisation properties of bentonite are studied. The laboratory part of the project consists of different test types e.g. fundamental swelling tests, measurement of friction between bentonite and other surfaces, homogenisation after loss of bentonite (the self-healing tests) and homogenisation in long tubes. Most tests have been run on a sodium dominated bentonite, but several of the tests have been repeated with a calcium dominated bentonite. In all tests de-ionized water was used.

The difference in homogenisation and sealing behaviour between the two bentonites have been analysed mainly from results in the fundamental series involving axial swelling between 10 % and 40 % and from the self-healing tests on homogenisation after loss of bentonite.

The tests, results and some of the diagrams are presented and described in detail in Dueck et al. (2014, 2016, 2018, 2022). Corresponding analyses were presented in the report by Dueck et al. (2019).

2.2 Material

The materials used are the sodium dominated Wyoming bentonite MX-80 (from American Coll. Co.) and the calcium dominated Calcigel (commercial bentonite from Clariant). Information about the materials can be found in e.g. Dueck et al. (2018) and Svensson et al. (2011). The water used was de-ionized water. For determination of void ratio and degree of saturation the particle densities ρ_s = 2 780 kg/m^3 and ρ_s = 2 695 kg/m^3 have been used together with the water density ρ_w = 1 000 kg/m^3.

2.3 Homogenisation after axial swelling

Fundamental swelling tests and self-healing tests have been made with both the sodium bentonite and the calcium bentonite, with results that can be compared. Some of these tests were done on specimens with the diameter 100 mm in a device shown with a sketch and a photo in Figure 2-1. Water was supplied from the upper side through a filter into the gap. When the measured swelling pressure was considered stable, the specimens were carefully dismantled and cut in slices for the determination of water content and density distributions.

In Figure 2-2 the results from all tests involving axial swelling and homogenisation in the HR-series are plotted with the average stress as a function of dry density, see also Table 2-1. The average stress is calculated according to Equation 2-1 from the stresses measured axially P_{axial} and radially P_{radial}. Results of MX-80 are shown to the left and results of Calcigel are shown to the right. The bars denote the maximum and minimum of the stresses and dry densities which thus illustrate the remaining inhomogeneity. It can be observed that in general larger differences between maximum and minimum dry density are seen in specimens of MX-80 while larger differences in stress are seen in the measurements on Calcigel. Two models are indicated in the diagrams, with references to SKB Technical Reports.

$$P_{average} = (P_{axial} + 2 \cdot P_{radial})/3 \quad (2\text{-}1)$$

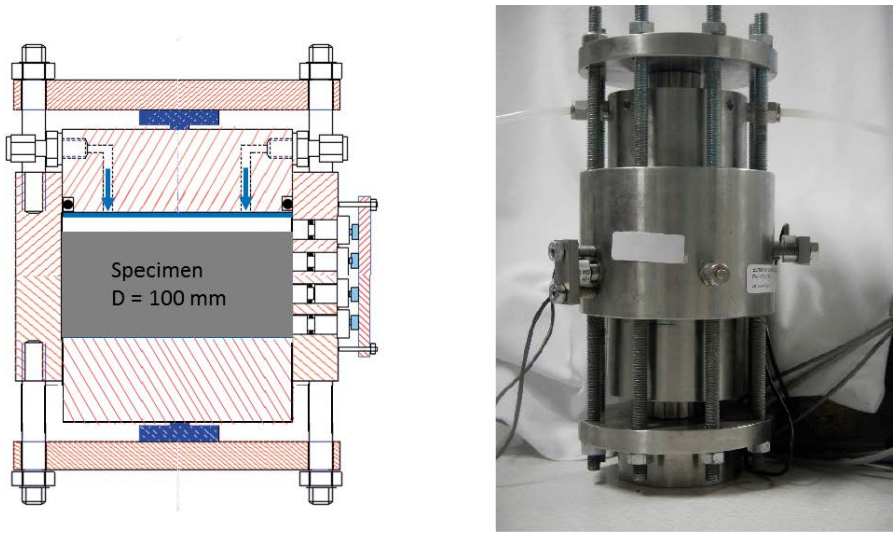

Figure 2-1. *Sketch and photo of the test equipment used for one of the series in the fundamental test series involving axial swelling. The specimens had an initial height between 50 and 60 mm while the initial gap was between 10 and 20 mm. The axial and radial stresses were measured with the load cells indicated in the sketch and water was added from above.*

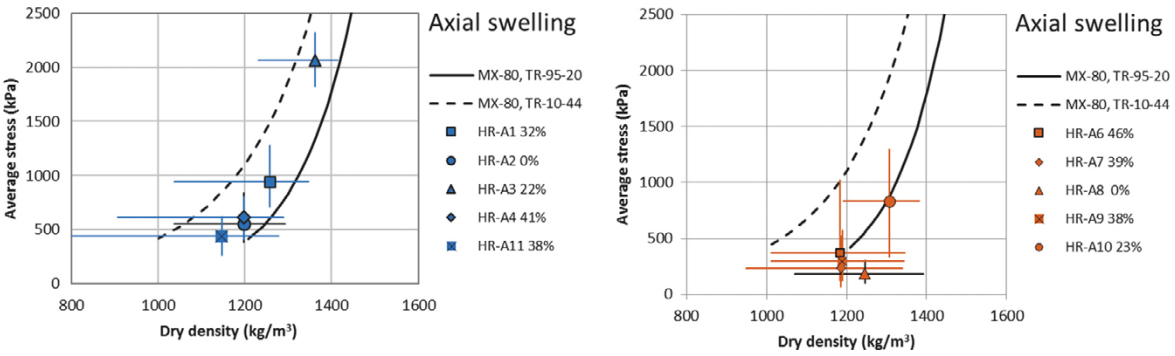

Figure 2-2. *Test results from all tests involving axial swelling in the HR-series. Results of MX-80 to the left and results of Calcigel to the right.*

Table 2-1. Test results from all tests involving axial swelling in the HR-series. The initial and final densities are indicated with the final height and the water pressure.

Sample ID	Material	ρ_{di} kg/m³	$\rho_{df,avr}$ kg/m³	Swell %	H_{final} mm	Time days	P_w kPa
HR-A1	MX-80	1 666	1 258	32	50	67	
HR-A2	MX-80	1 232	1 198	0	50	72	
HR-A3	MX-80	1 666	1 362	22	50	70	
HR-A4	MX-80	1 693	1 197	41	70	145	
HR-A6	Calcigel	1 730	1 185	46	70	117	
HR-A7	Calcigel	1 644	1 186	39	70	173	500
HR-A8	Calcigel	1 169	1 246	0	70	129	100
HR-A9	Calcigel	1 647	1 190	38	70	133	100
HR-A10	Calcigel	1 581	1 307	23	70	179	500
HR-A11	MX-80	1 583	1 147	38	70	145	200

The density distributions of all specimens in the HR-series that swelled into an empty void are shown in Figure 2-3. These diagrams illustrate once again that the largest differences in dry density are observed in specimens of MX-80. In addition, it can also be observed that the largest gradient in dry density of the MX-80 specimens is seen in the upper part while the corresponding largest gradient of the Calcigel specimens is present in the middle of the specimens.

To be able to compare results from specimens with different initial dry density the density distributions were normalized with the initial dry density according to Figure 2-4. In the diagrams the amount of swelling (20–30 %, 30–37 %, 38–46 %) is marked with different colours (brown, orange, yellow). Results of MX-80 and Calcigel are shown to the left and right, respectively.

Previously, similar test series were run in a smaller scale, with the diameter 50 mm and the height 25–28 mm. The series were later replaced by the HR-series to get higher resolution in the distribution of base variables over the specimens. Resulting density distributions after axial swelling in the smaller scale tests are shown in Figure 2-5. In these diagrams the normalized density distributions are shown with results of MX-80 to the left and of Calcigel to the right. The amount of swelling (0–10 %, 10–20 %, 20–30 %, 30–37 %) is marked with the colours (blue, green, brown, orange), in agreement with Figure 2-4.

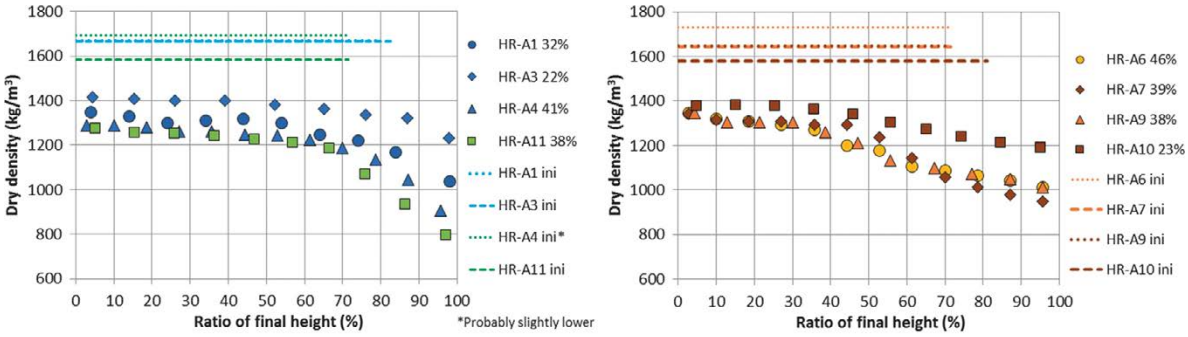

Figure 2-3. *Density distributions of specimens that swelled into an open space in the HR-series involving axial swelling. Results of MX-80 to the left and results of Calcigel to the right.*

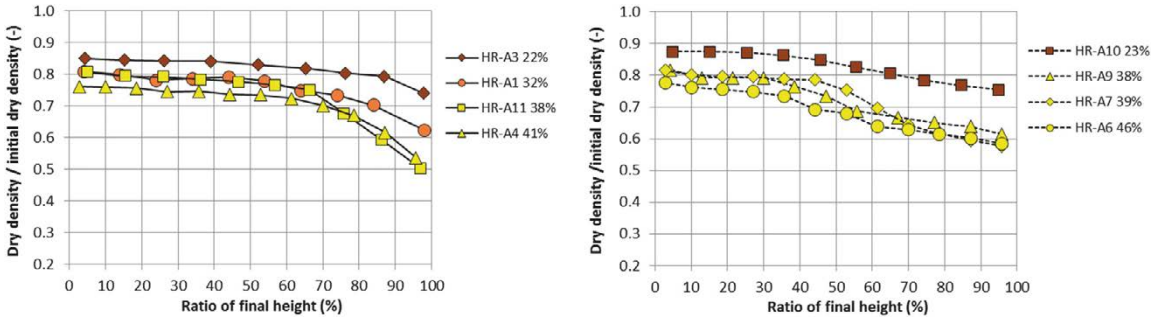

Figure 2-4. *Normalized density distributions as a function of height (i.e. the ratio of height) from the tests in the HR-series and Figure 2-3. Results of MX-80 to the left and Calcigel to the right. Different colours are used for different amounts of swelling.*

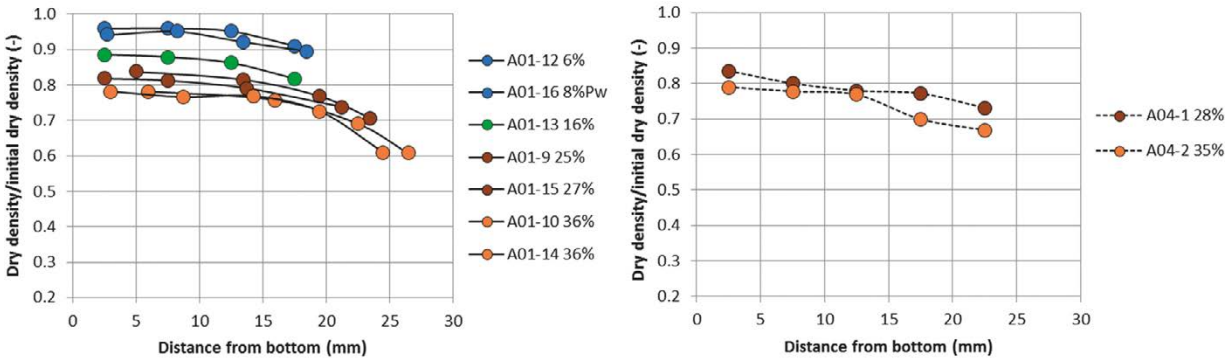

Figure 2-5. *Density distributions normalized with the initial dry density is plotted as a function of distance from the bottom. Results of MX-80 to the left and results of Calcigel to the right. Different colours are used for different amounts of swelling but in agreement with Figure 2-4.*

The results in the two scales shown in Figure 2-4 and Figure 2-5 are consistent. The diagrams show that larger swelling gives larger density gradients and in general less gradients in Calcigel compared to MX-80.

In some tests in the HR-series water pressure of 100–500 kPa was applied, which should be commented. The only test on MX-80 with water pressure was HR-A11. No large influence on the density gradient was seen when comparing with the HR-A4 exposed to larger but comparable swelling. On Calcigel, water pressure was applied in all tests but one, HR-A6. Since this specimen HR-A6 was the one that homogenised the most, despite it swelled the most and was run shortest time, the influence of water pressure cannot be considered as decisive.

One test of each material was run on specimens that did not swell into an empty void but homogenised from initial differences in density. In the tests HR-A2 (MX-80) and HR-A8 (Calcigel), two samples of the same material but with different dry density were put together to fill out the total height and diameter of the device. The results are shown in Figure 2-6.

There were some differences between the two tests in that the average dry density was not the same and different initial water contents were used. The average dry density of the specimen used in HR-A2 (MX-80) was 1 200 kg/m^3 while the average dry density of the specimen used in HR-A8 (Calcigel) was 1 245 kg/m^3. The initial water content was constant over the height of the MX-80 specimen (24 %) while different water contents were used in the upper and lower part of the Calcigel specimen (64 % and 32 %, respectively). In these two tests (HR-A2 and HR-A8) the average dry density should be the same at mounting and at dismantling which was approximately achieved in HR-A2 while larger difference was seen in the results from HR-A8 where the initial dry density must be considered as uncertain.

The results from the specimen exposed to only homogenisation, i.e. without any open void, showed some differences compared to the results after swelling into an open void with subsequent homogenisation. For MX-80 the difference in dry density over the specimen height was less when exposed to only homogenisation compared to when exposed to swelling with subsequent homogenisation while the difference in stress was approximately the same and irrespective of test type. Comparing the specimens of Calcigel the dry density distribution over the specimen height was approximately the same and irrespective of swelling into a void or not, but the difference in stress was much less when exposed to homogenisation without swelling into a void.

Comparing the specimens of MX-80 and Calcigel after homogenisation without any open void, the difference in dry density was larger over the specimen of Calcigel even though the difference in stress was less over this specimen. This is in contrast to the results after swelling with subsequent homogenisation. However, in spite of the high average dry density of the Calcigel specimen, the measured stresses were much lower, which is logical at the presence of very low densities. Further reference tests on Calcigel could give valuable information to be used for the analyses of the behaviour after large swelling.

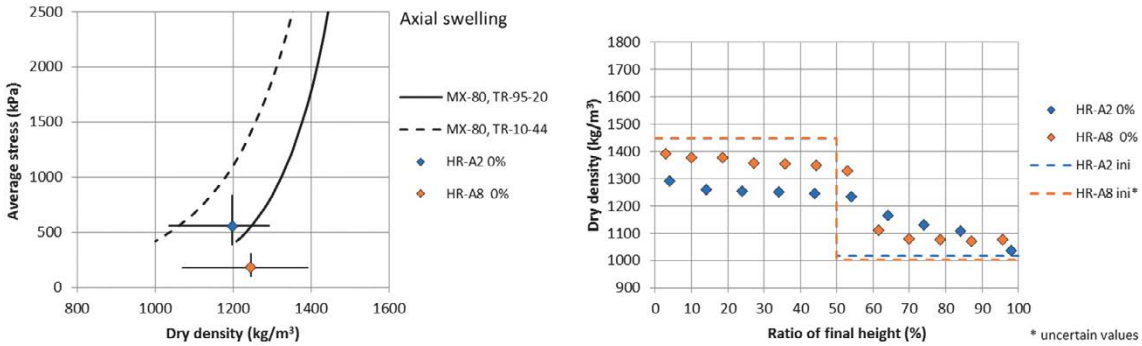

Figure 2-6. *Results from two specimens exposed to homogenisation without swelling into an open void; HR-A2 (MX-80) and HR-A8 (Calcigel). Average stress as a function of dry density to the left and dry density as a function of height to the right.*

The maximum stress and dry density from each test on MX-80 represent a trend line corresponding to the solid blue line to the left in Figure 2-7 and the minimum values are represented by the green solid line. The corresponding lines representing maximum and minimum values of Calcigel are plotted with brown and orange lines, respectively, to the right in Figure 2-7.

The conditions along the lines representing maximum and minimum values might be interpreted as swelling at unloading and consolidation at loading, respectively which both seems to be present within the analyzed specimens. The resulting larger density gradient of MX-80 than of Calcigel when swelling into an open void can perhaps be explained by difference in stress paths. MX-80 expands to a very low density at first, which is followed by consolidation, while Calcigel swells to the final condition without consolidation.

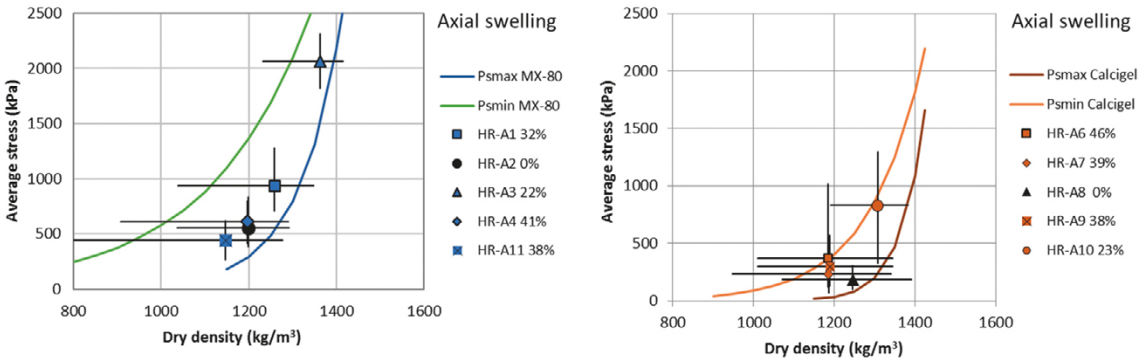

Figure 2-7. *Results from all tests involving axial swelling in the HR-series plotted with average stress as a function of dry density. Results from tests on MX-80 to the left and on Calcigel to the right. The bars show maximum and minimum dry densities and stresses of the specimens and thus illustrate the remaining inhomogeneity. Lines representing the maximum (blue and brown) and minimum (green and orange) conditions are plotted.*

2.4 Homogenisation after loss of bentonite

The self-healing tests, with healing of two cavities cut in a bentonite ring, were done on rings with the diameter 300 mm and height 100 mm. The two cavities cut out at diametrical positions of the bentonite ring had the height 35 mm, length 70 mm and depth 50 mm. In Figure 2-8 a sketch and a photo of a bentonite ring used in the self-healing tests are shown. Water was supplied from the periphery of the devices through a radial filter.

The completed self-healing test SH1 was run with MX-80 while the also completed test SH3 was run with Calcigel. Both bentonite blocks were close to water saturation at start with the initial dry density 1 618 kg/m^3 and 1 662 kg/m^3 for SH1 and SH3, respectively. While SH1 was instrumented and run for 33 months SH3 had no instruments and was run for 44 months.

In Table 2-2 the dry density of each specimen is given at three conditions; at compaction, initially at test start and at dismantling. The three densities are based on the initial dry mass and the volume at compaction, the initial dry mass and the volume to fill the device and finally the dry mass after removing the bentonite in the cavities and the volume to fill the device.

Table 2-2. Conditions of the specimens used in tests SH1 and SH3.

SH-test	Material	At compaction dry density kg/m^3	Initial condition dry density kg/m^3	water content %	saturation %	Final average dry density kg/m^3
SH1	MX-80	1 642	1 618	24.2	94	1 568
SH3	Calcigel	1 685	1 662	21.7	98	1 589

The blocks in SH1 and SH3 were carefully sampled and the radial dry density distributions measured at three levels of the bentonite blocks (outermost, second outermost and innermost) according to Figure 2-9. The results are shown in Figure 2-10 to Figure 2-12, to the left and right, respectively. The dry densities were calculated from bulk densities and water contents determined on the upper and lower part, respectively, at corresponding positions. Thus, symmetry between the upper and lower parts was used, which was also studied and considered to be approximately fulfilled. In addition, the determined degree of saturation was calculated to approximately 100 % over the blocks.

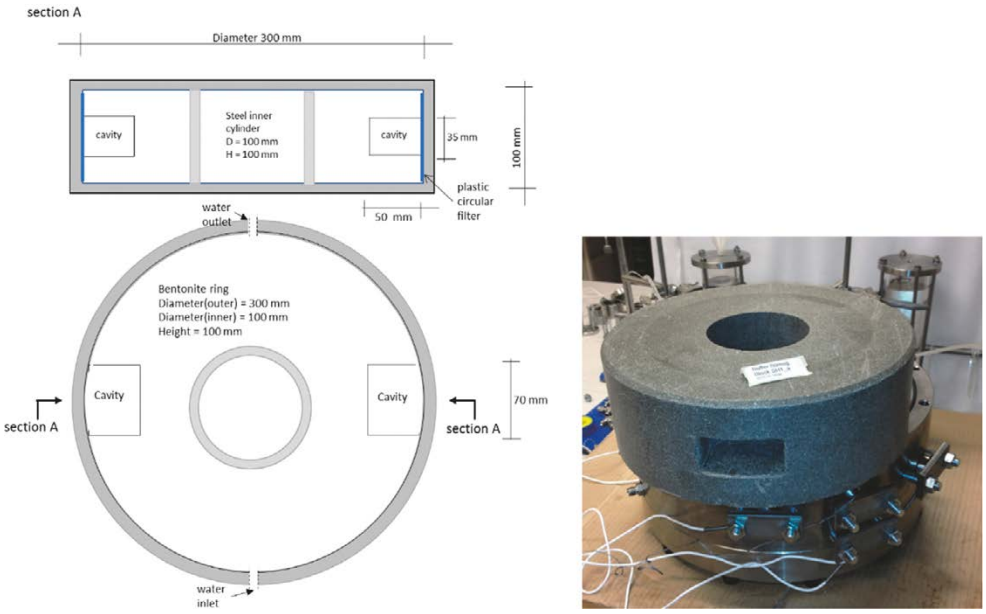

Figure 2-8. *Sketch and photo of the test equipment used for one of the tests in the self-healing series involving sealing of two large cavities cut out at diametrical positions of a bentonite ring. The bentonite ring had the outer diameter 300 mm, the inner diameter 100 mm and the height 100 mm.*

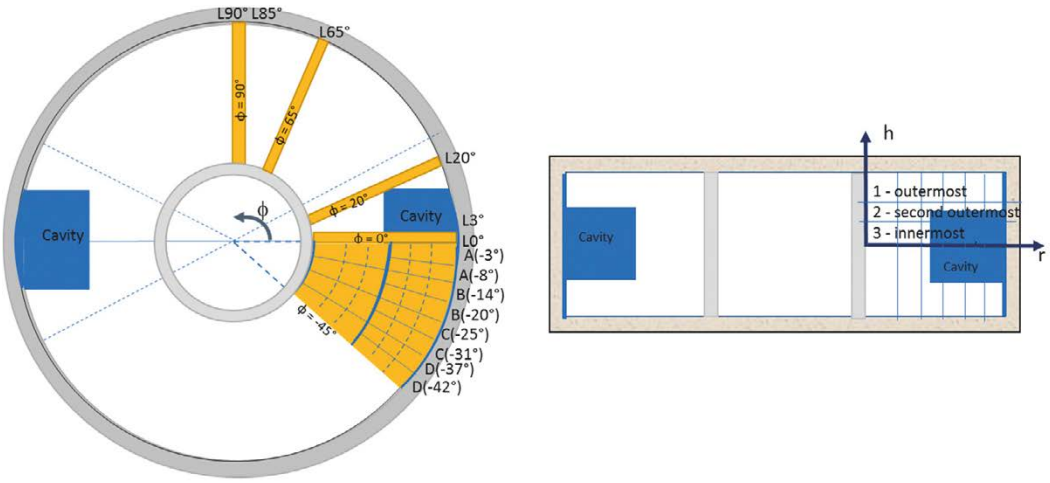

Figure 2-9. *Plan view (to the left) which shows the sampling along lines at different angles between 0° and 90°, from the centre of the cavity, and the continuous sampling within a sector between 0° and –45°. The section (to the right) shows the different axial levels for the sampling; outermost, second outermost and innermost.*

The different colours (red, brown, orange, yellow, green, blue, purple and black) indicate the sampling lines at different angles, between 90° and −42°, from the centre of the cavity. The small illustration in the diagrams illustrates the locations of the sampling lines. The cavities are marked with blue rectangles.

The initial and final dry densities from Table 2-2 are marked with plus signs at zero radial distance; the upper sign is the initial value and the lower represents the final average dry density. The final average values of the dry density were also estimated after the dismantling and the values agreed well with the previous calculated values, ± 10 kg/m^3.

The lowest densities (yellow and green marks) and the highest densites (red marks) were seen in the directions coinciding with and perpendicular to the direction of the cavity, respectively, in both blocks.

The results indicate that the dry density differences were less in Calcigel compared to in MX-80. Somewhat longer time was used for the Calcigel test (3.7 years) compared to the MX-80 test (2.8 years).

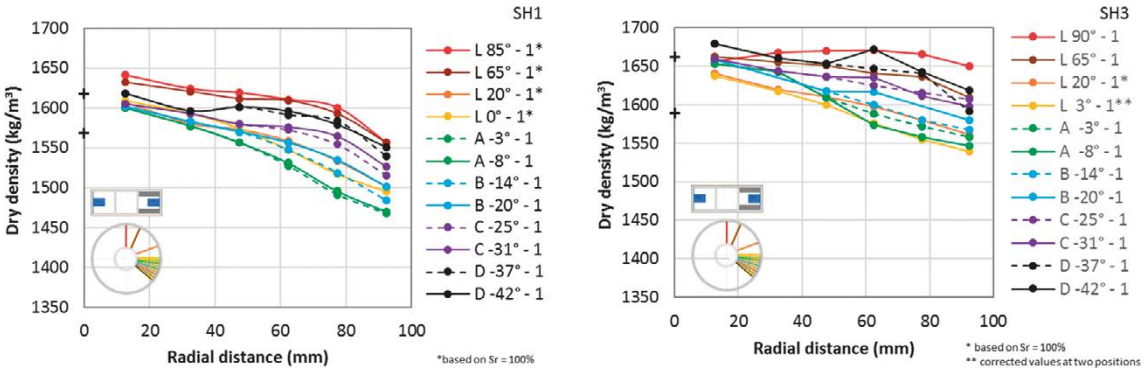

Figure 2-10. *Distribution of dry density at the outermost level 1 in different directions. Results of MX-80 (SH1) to the left and of Calcigel (SH3) to the right. The colours (red, brown, orange, yellow, green, blue, purple, black) show angles between +90° to –42° from the centre of the initial cavity. The angles are indicated in the labels. The initial and final average conditions are marked with plus signs. The locations of level 1 and the different directions are shown to the lower left in the diagrams.*

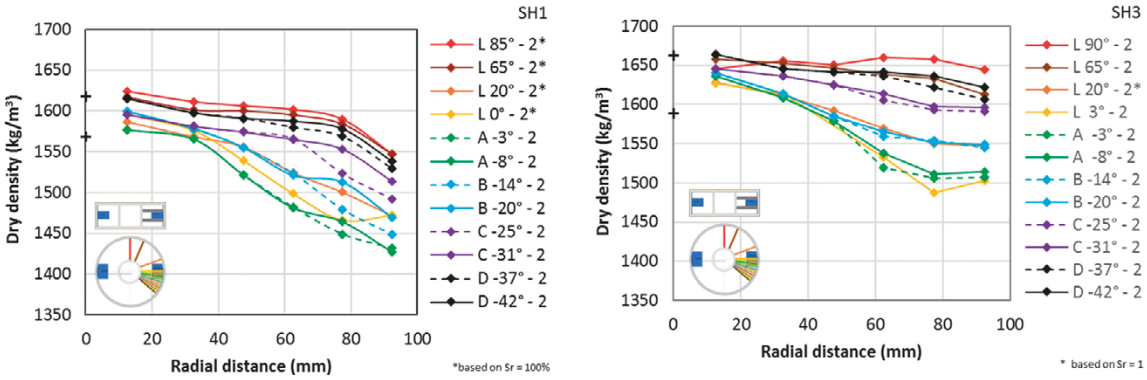

Figure 2-11. *Distribution of dry density at the second outermost level 2 in different directions. Results of MX-80 (SH1) to the left and of Calcigel (SH3) to the right. See Figure 2-10 for description of the labels and marks. The locations of level 2 and the different directions are shown to the lower left in the diagrams.*

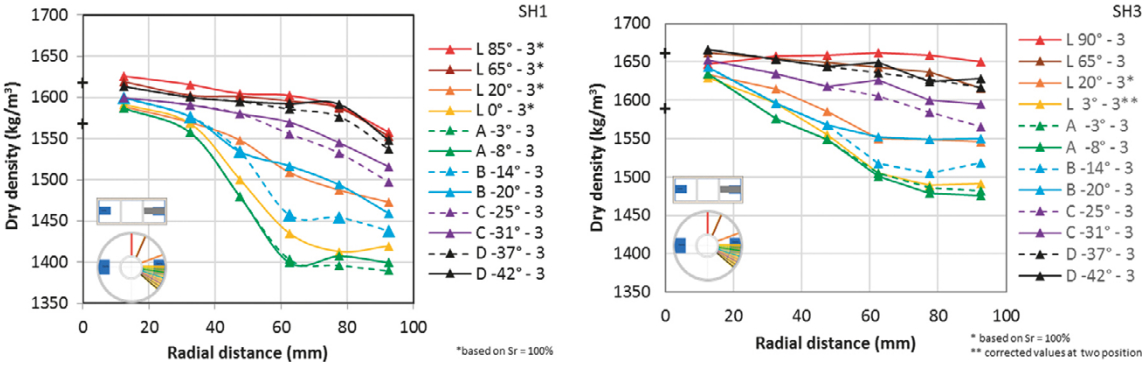

Figure 2-12. *Distribution of dry density at the innermost level 3 in different directions. Results of MX-80 (SH1) to the left and of Calcigel (SH3) to the right. See Figure 2-10 for description of the labels and marks. The locations of level 3 and the different directions are shown to the lower left in the diagrams.*

2.5 Concluding remarks

The difference in homogenisation and sealing behaviour between the Ca-bentonite and the Na-bentonite have been analysed from tests involving axial swelling into an initial gap and swelling into a larger cavity.

From the analysis a very similar homogenisation behaviour was seen for the two bentonite types. After swelling and at comparable conditions somewhat less density differences were observed in the Ca-benonite, which thus was more homogenised. The observations were based on results after swelling into larger voids in the SH-series and after axial swelling in the HR-series.

Several reference tests have been run on MX-80 and additional reference tests on Calcigel could be useful for further comparison and analyse of homogenisation of specimens of Calcigel.

3 Comparison of homogenisation and sealing behaviour after rapid and slow water uptake

3.1 General

Presently an SKB project is running where the self-sealing and homogenisation properties of bentonite are studied. The laboratory part of the project consists of different test types, e.g. fundamental swelling tests, measurement of friction between bentonite and other surfaces, homogenisation after loss of bentonite and homogenisation in long tubes.

Buffer homogenisation involving loss of bentonite has been studied by medium scale laboratory tests, called the self-healing tests (SH). Four tests have been started and all of them have been finished and dismantled after testing periods between 17 and 44 months. The circular blocks used for the tests had the same geometry, i.e. the height and diameter were the same and the cavities cut out in the blocks before the tests were approximately of the same size. While Wyoming Na-bentonite was used for three of the tests (SH1, SH2 and SH4) one test was run on a Ca-bentonite (SH3). The results have been reported in status reports of the project (Dueck et al. 2016, 2018, 2022).

In one of the tests, SH4, water was supplied at a limited and slow inflow rate while water was added unlimited in the other tests in the series. The impact of the slow water uptake on stress and density distributions has been analysed by comparing the test results from SH4 with the test results from other tests in the series. A comparison between SH4 and SH1 is particularly suitable since these tests were both instrumented with load cells, the same type of bentonite was used, and the cavities cut out in the blocks were of the same size. However, the initial degree of saturation was different and also the total testing time.

3.2 Material

The material used is the sodium dominated Wyoming bentonite Volclay MX-80 (from American Coll. Co). Properties of the material are presented by e.g. Karnland et al. (2006) and Svensson et al. (2011). De-ionized water was used for the saturation. For determination of void ratio and degree of saturation the particle densities ρ_s = 2 780 kg/m^3 and the water density ρ_w = 1 000 kg/m^3 have been used.

3.3 Experiment description

The geometry of the set-up used in the series is shown in the sketch to the left in Figure 3-1. The containment is a very stiff cylinder with the inner diameter 300 mm and the height 100 mm. An inner cylinder with the outer diameter 100 mm is included in the centre. A stiff filter is mounted to the inside of the outer ring with the purpose to provide water to the bentonite from the inlet on the radial surface. In each bentonite block two cavities were cut out in two diametrical positions in order to simulate loss of material. Nine load cells for measuring swelling pressure were included in the set-up. The positions of the sensors used in the tests are shown to the right in Figure 3-1.

After preparation of the bentonite rings, cutting the cavities and installing the load cells water was added. In three of the tests the water was filled into the filter and tubes and a water pressure of approximately 10 kPa was applied. In test SH4 the water was supplied with a controlled flow rate of 0.072 ml/h to saturate the block slowly in two years.

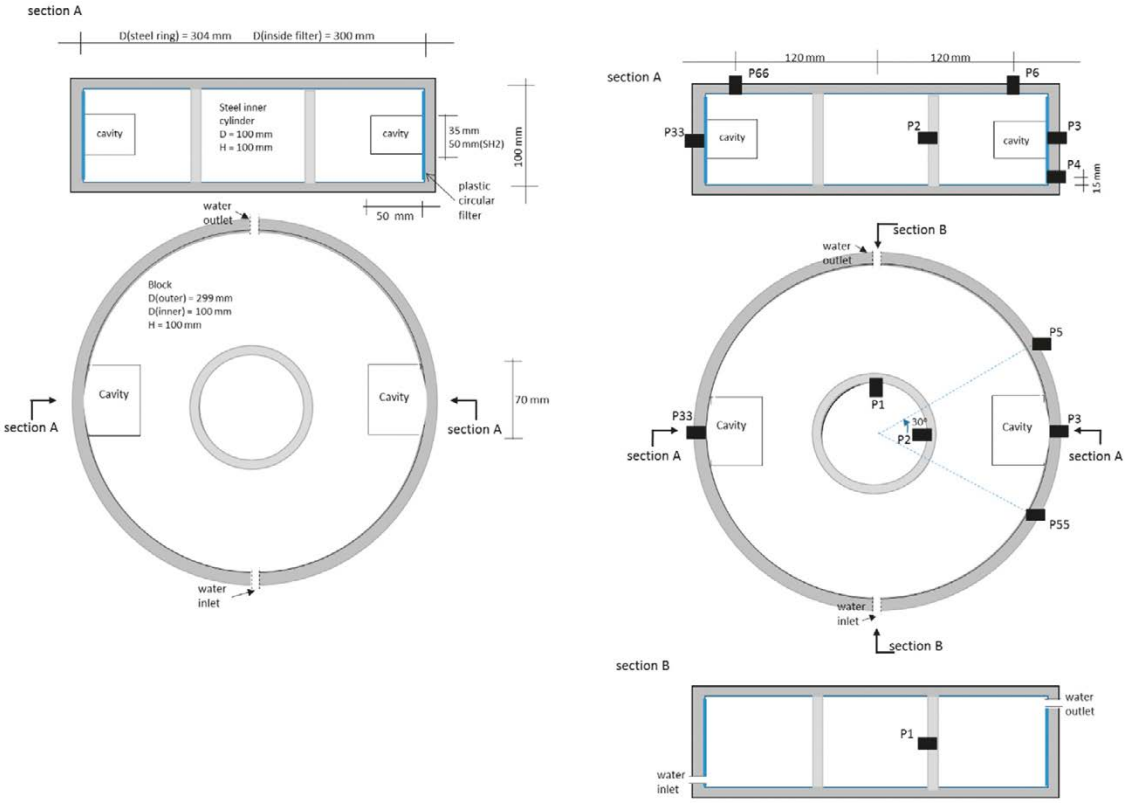

Figure 3-1. *A sketch of the set-up used for the self-healing tests (to the left) and a sketch showing the positions of the sensors used in test SH1 and SH4 (to the right). The dimensions of the outer and inner steel cylinders and the bentonite block with the cavities are shown as well as the plastic filters and the locations of the water inlet and outlet.*

3.4 Results and comparison

The blocks were installed with the initial dry density 1 618 kg/m^3 and 1 636 kg/m^3 for the tests SH1 and SH4, respectively. In Table 3-1 the dry density of each specimen is given at three conditions; at compaction, initially at test start and at dismantling. The three densities are based on the initial mass and the volume at compaction, the initial mass and the volume to fill the device and finally the dry mass after removal of the cavities and the volume to fill the device. The initial degree of saturation differed according to Table 3-1. The tests SH1 and SH4 were terminated after 33 and 43 months, respectively.

Table 3-1. Conditions of the blocks used in the tests SH1 and SH4.

SH-test	Material	At compaction dry density kg/m^3	Initial condition dry density kg/m^3	water content %	saturation %	Final average dry density kg/m^3
SH1	MX-80	1642	1618	24.2	94	1568
SH4	MX-80	1655	1636	16.5	65	1563

The water pressure measured at the water inlet in the two tests are shown in Figure 3-2. In SH1 the degree of saturation was high from start and the block was almost saturated a couple of days after the start of the test. The water supply was open during the entire course of the test with a constant water pressure of 100 kPa applied after 20 days and then kept constant, see Figure 3-2 to the left. Since no indication of loss of water was observed or measured the pressure was assumed to be constant everywhere in the filter.

In test SH4 the controlled water inflow was applied from start. The evolution of the water pressure at the inflow is shown in Figure 3-2 to the right. The water pressure increased during the test and after approximately three years, seven months before the termination, the water pressure was limited to 400 kPa and the flow control was changed to water pressure control. A leakage was detected, located above the water outlet between the lid and the confining ring, and the pressure applied at the inflow side was probably not kept everywhere in the filter. During the last part of the test the pressure was measured at the outlet to be 55 kPa. In both SH1 and SH4 the water pressure was lowered to zero five days before dismantling.

In Figure 3-3 the swelling pressure measured in the two tests are shown, presented as the evolution of total stress with time. The sensors were located at the same positions in the two tests and the colours used for the sensors are the same.

As shown in Figure 3-3 the maximum and minimum final values of the swelling pressure in the two tests were approximately the same. However, the evolution with time was quite different and while the swelling pressure in SH1 increased rapidly during the first months and reached final values more or less after one year, the final values of SH4 were not reached until after 2.5 years.

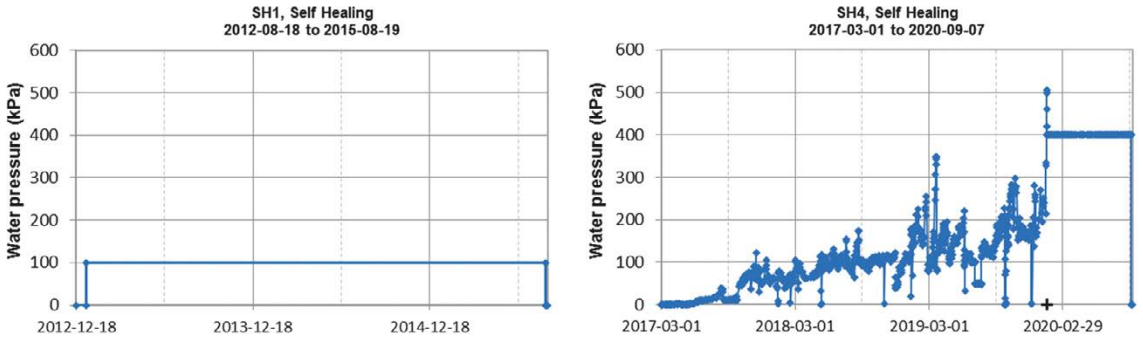

Figure 3-2. *Controlled water pressure in test SH1 (to the left) and water pressure build-up at control of water inflow in test SH4 (to the right). In test SH4 the water pressure was controlled to 400 kPa during the last months of the test.*

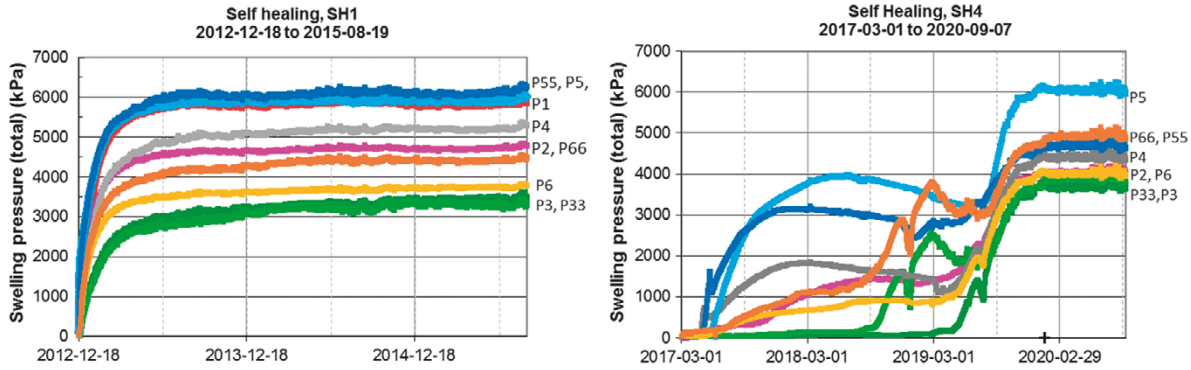

Figure 3-3. *The evolutions of total stress with time measured in test SH1 (to the left) and SH4 (to the right). The positions, numbers and colours of each sensor are the same in the two tests.*

Comparing final values, the swelling pressure measured in the initial cavities, sensors P3 and P33, were approximately the same in both tests although a little higher in SH4. However, the values registered by sensors P5 and P55 (on opposite sides of one of the cavities) were approximately the same in SH1 but different in SH4. This indicates a non-symmetrical behaviour in test SH4 where larger swelling pressure (6 000 kPa) was measured towards the outlet compared to towards the inlet (4 500 kPa). In both tests there is a difference between P6 and P66 (in the lid) however larger difference in SH4. Since the stresses are shown as total stresses there might also be an influence of the water pressure which at least in the filter of SH1 was larger than in SH4.

The tests SH1 and SH4 were finished after 33 and 43 months, respectively. Slightly different techniques were used for the dismantling, but this was not considered to influence the sampling and the measured water content and density distributions. While the block used in SH4 was forced out of the cylinder ring by a hydraulic jack the block in SH1 was removed by free drilling, removal of the inner steel cylinder and dismantling of one half of the cylinder at a time.

The main type of sampling of the blocks in this series was made along lines and continuously within a sector, illustrated in Figure 3-4. The sampling was made with an assumption that the upper and lower parts were symmetrical. The density was determined on the upper part and the water content at the corresponding position in the lower part. All determinations were made in three levels; outermost, second outermost and innermost.

Sampling along lines were made at angles 90°, 65°, 20°, 0°, –65° and –90° from the centre of the cavity and continuously within a sector between –45° and 0°. The size of the specimens was approximately $15 \times 15 \times 15$ mm^3.

The distributions of dry density after dismantling of the two blocks are shown in Figure 3-5 to Figure 3-7. The colours (red, brown, orange, yellow, green, light blue, lilac and black, light grey and dark grey) indicate the angles from the cavity (90°, 65°, 20°, 0°, –6°, –17°, –28°, –39°, –65°, –90°) The same colours are used in the results from SH1 and SH4. However, sampling along the lines at the angles –65° and –90° was only made in SH4 due to the indications of non-symmetrical behaviour. The locations of the levels and the directions are indicated to the lower left in the diagrams.

The lowest densities (green) and the highest densities (red) were in both tests seen in the direction coinciding with and perpendicular to the direction of the cavity. When the densities at different levels (outermost, second outermost and innermost) are compared decreasing values are generally shown, which is logical. Both blocks were water saturated at dismantling.

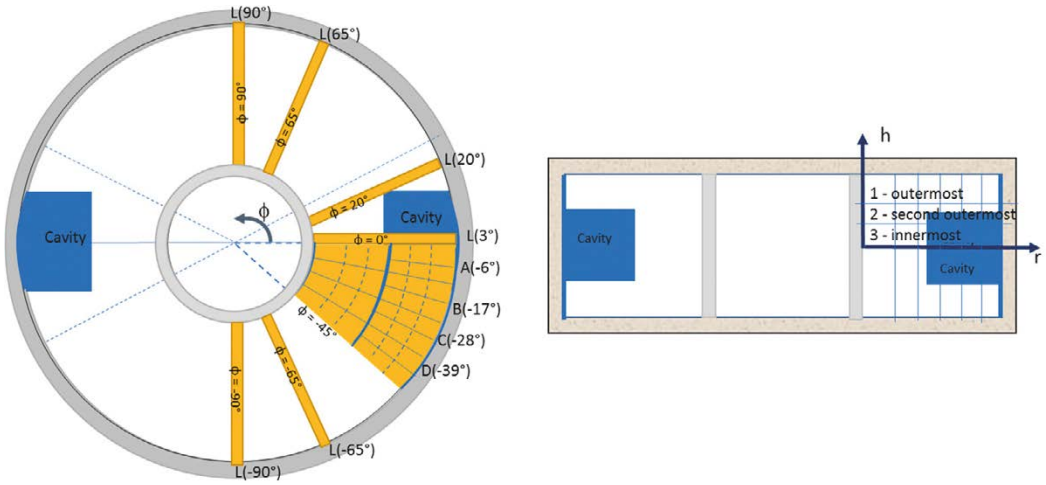

Figure 3-4. *Plan view (to the left) which shows the sampling along lines at different angles from the middle of the cavity; 90°, 65°, 20°, 0°, –65° and –90° and the continuous sampling within a sector between 0° and –45°.The section (to the right) shows the different axial levels for the sampling; outermost, second outermost and innermost.*

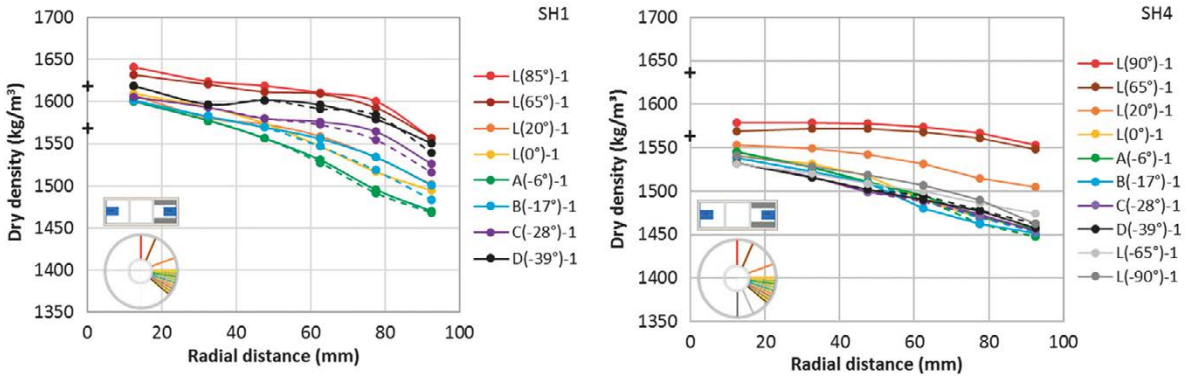

Figure 3-5. *Distribution of dry density at the outermost level 1 in different directions. The colours (red, brown, orange, yellow, green, light blue, lilac, black, light grey, dark grey) indicate different angles (90°, 65°, 20°, 0°, –6°, –17°, –28°, –39°, –65°, –90°) from the centre of the initial cavity. The upper plus sign indicates the initial dry density and the lower indicates the final dry density from Table 3-1.*

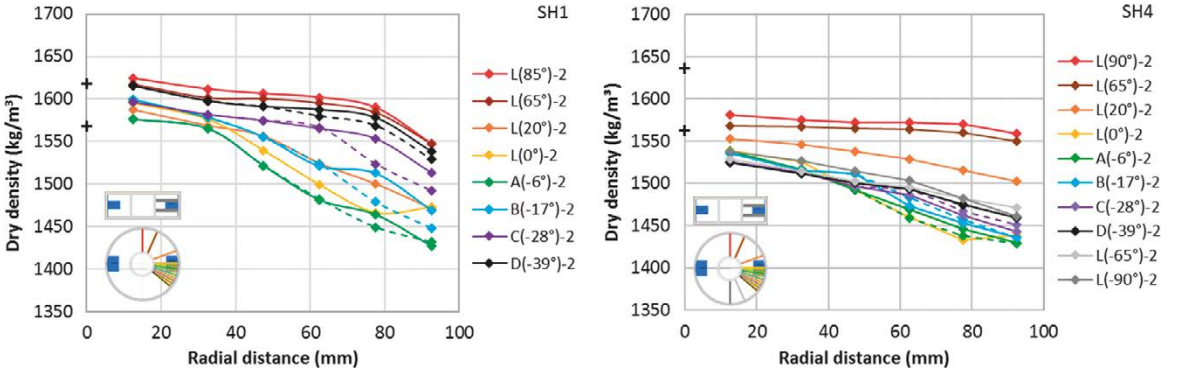

Figure 3-6. *Distribution of dry density at the second outermost level 2 in different directions. The colours and the plus signs are the same as in Figure 3-5.*

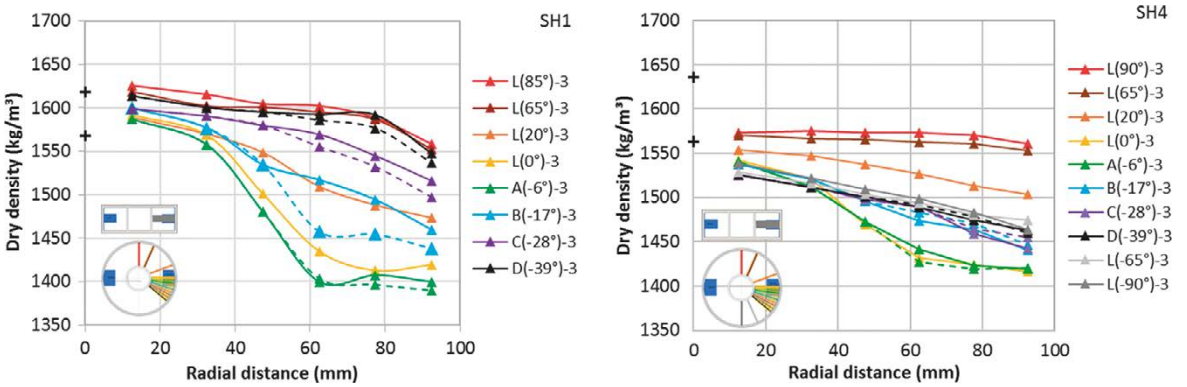

Figure 3-7. *Distribution of dry density at the innermost level 3 in different directions. The colours and the plus signs are the same as in Figure 3-5.*

In Figure 3-5 to Figure 3-7 the initial and final dry density from Table 3-1 are indicated with an upper and lower plus sign at zero radial distance. The dry density after dismantling SH4 was in all positions lower than the initial dry density, which was not the case in the results from SH1. The difference between initial dry density and the final average dry density (the distance between the plus signs) in the two tests should have been the same but is slightly larger in SH4 which indicates some uncertainties in the average densities. The difference is even larger if the weighted average of the dry density after dismantling is used (1 556 kg/m^3 and 1 526 kg/m^3 for SH1 and SH4, respectively).

The dry density gradients in SH1 and SH4 differ. Smaller gradients are in general seen in the results from SH4. The relatively low density at the angle 90° (red line) at the distance 92 mm in SH1 is not seen in SH4. The steep gradients at the innermost level at the centre of the cavity is also not seen in SH4.

The densities at the angles +65° and –39° (brown and black lines, respectively) in SH1 indicate increasing densities from the cavities towards both water inlet and outlet and thus, that the behaviour is symmetrical on different sides of the cavities. However, in SH4 the resulting dry densities at the angle –90°, –65° and -39° all coincide and do not increase towards the water inflow. This indicates a non-symmetrical behaviour not seen in SH1 but indicated also by the swelling pressure above.

Symmetry between the upper and lower part was assumed at sampling and the bulk density was determined on the upper part and the water content on the lower part. The symmetry between the upper and lower parts was analysed in the two blocks by determination of bulk density in both the upper and lower parts, along a line. The differences between corresponding position in the upper and lower parts was less than 20 kg/m^3 in SH1 and less than 50 kg/m^3 in SH4. The difference indicates some uncertainties in the determinations. Further sampling, if possible, might give additional information.

3.5 Concluding remarks

The difference in water uptake rate and the difference in initial water content did not influence the maximum and minimum swelling pressure. However, in the test results of SH4 where water was added slowly, swelling took placed at all positions and the density gradients were in general lower than in the test results from SH1, where the water supply was unlimited from start and the initial degree of saturation was higher. In addition, a non-symmetrical behaviour was seen in the results from SH4 in that larger swelling took place towards the water inlet. This could be observed both in the swelling pressure and in the density distribution.

The two tests differ both regarding initial degree of saturation and wetting history. It is probable that the non-symmetrical behaviour observed after wetting and homogenisation being completed was caused by the slow and non-symmetrical water supply since swelling starts at the water inlet point, which will cause local swelling and possible displacement of the block. However, the lower density gradients observed in the slowly wetted test may have been caused by both the initially lower degree of saturation and the slow wetting.

4 Comparison of homogenisation of bentonite in long steel tubes after two, four and six years

4.1 General

Presently an SKB project is running where the self-sealing and homogenisation properties of bentonite are studied. The laboratory part of the project consists of different types of tests, e.g. fundamental swelling tests, measurement of friction between bentonite and other surfaces, homogenisation after loss of bentonite and homogenisation in long tubes.

One important part of this project consists of long-time homogenisation tests in steel tubes. The purpose of these tests is to study the effect of friction for limiting homogenisation and also to study the influence of time on the remaining density gradients after completed swelling and compression. The results can also be applied to evaluate to what extent the so called “transition zones” in tunnels can be used to downshift the swelling pressure against e.g. a plug.

By using different test durations before termination and sampling, the influence of time and creep on the distribution of density can be studied. Three tests have been finished after 2, 4 and 6 years while seven are still ongoing. A comprehensive description of the tests and results can be found in Dueck et al. (2018, 2022).

The results are analysed by an analytical model based on force equilibrium after pore pressure equilibrium which includes the friction between the bentonite and the side walls. A friction angle has been be evaluated from the measured length of the transition zone and the measured swelling pressures.

4.2 Material

The materials used are the sodium dominated Wyoming bentonite MX-80 (from American Coll. Co.) more information can be found in e.g. Karnland et al. (2006). De-ionized water was used for the saturation. For determination of void ratio and degree of saturation the particle densities ρ_s = 2 780 kg/m^3 and the water density ρ_w = 1 000 kg/m^3 have been used.

4.3 Experiment description

Ten long tubes with similar design and content of bentonite, FLR1-FLR10, have been used. The length of the tubes is 250–350 mm and the diameter is 25–35 mm. The inner surface of 9 tubes was machined to be grooved and thus very raw. The lower half of each tube is filled with highly compacted MX-80 bentonite and the upper half is filled with MX-80 pellets. Water is freely available from the upper end through a filter above the pellets. In some of the devices, stresses are measured radially or axially at 4 positions. In Figure 4-1 a sketch and a photo of the set-up are shown.

In Figure 4-2 the most common set-up, used in tests FLR2 and FLR5-10, is shown in more detail. The type of grooves used inside these tubes are also shown. The other set-up differs in that FLR1 has slightly different grooves and different distance between radial stress measurements, FLR3 has a smooth inner steel wall towards the bentonite and FLR4 has a different geometry.

At test start a 2 mM NaCl-solution was added after air evacuation of filters, tubes and devices. After this, the calculated degree of saturation was approximately 100 % in all tubes. After a couple of weeks, the solution was changed to 50 mM NaCl. FLR2-FLR10 started in May 2013 while FLR1 started in 2012. A constant water pressure of 70 kPa was applied on all specimens in October 2015, except FRL1 (where water pressure was applied some months later) and FLR5 (where no pressure was applied before termination).

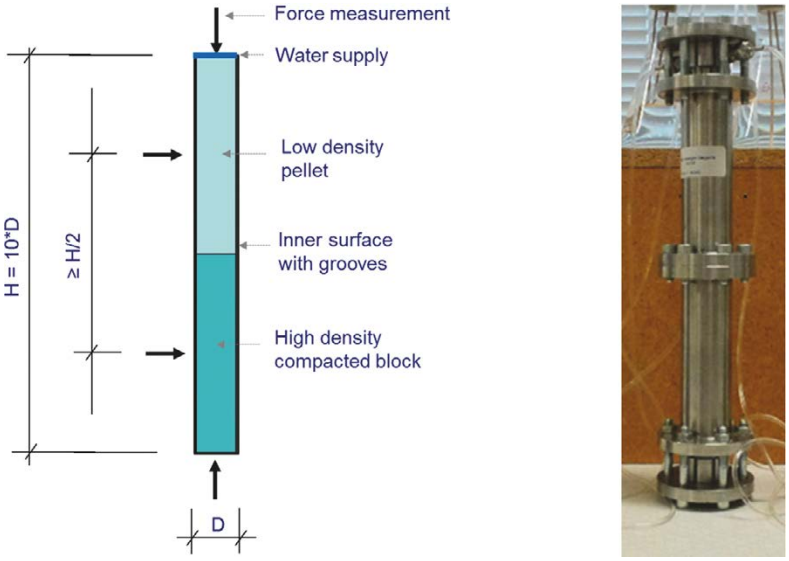

Figure 4-1. *Sketch and photo of the Long Steel Tubes used in the test series. Axial and radial stress measurements are made in some of the tubes (marked with arrows).*

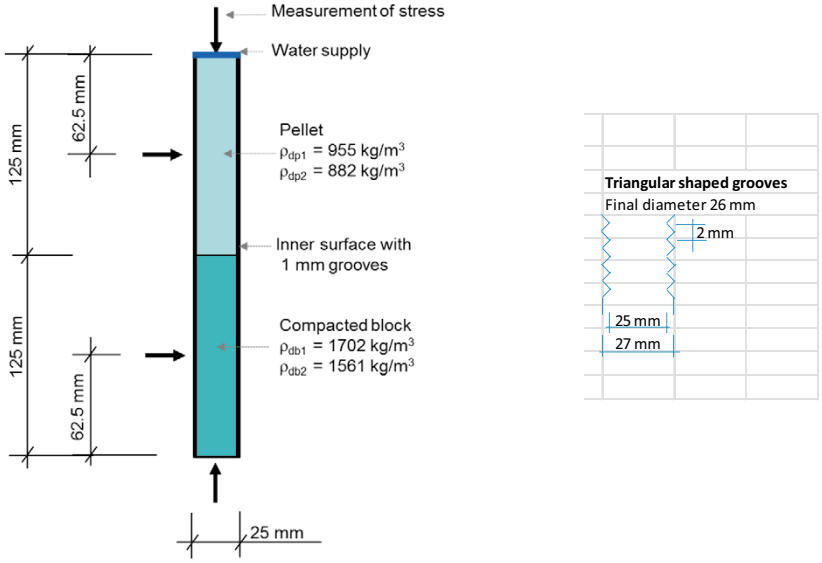

Figure 4-2. *Sketch with distances and densities of FLR2.The set-up was also used for FLR5-FLR10 but then without the stress measurements. The grooves inside the mentioned tubes are shown to the right.*

4.4 Resulting measurements

Three tests have been finished FLR5, FLR6 and FLR7 after 2, 4 and 6 years, respectively. The resulting dry density distributions are shown in Figure 4-3 and Table 4-1. In Figure 4-3 (to the left) the measured dry density is shown but since the average dry density of the three terminated tests differed slightly, Table 4-1, the results are also plotted as normalized dry density to the right. The dry density was normalized with the ratio of the actual average density to the average dry density (1 255 kg/m^3) of all three terminated tests.

Table 4-1. Results from FLR5-FLR7. The total time are given together with values of average dry density.

Sample ID	FLR5	FLR6	FLR7
Start date	2013-05-15	2013-05-16	2013-05-16
End of test	2015-05-20	2017-05-29	2019-05-02
Total time	2 years	4 years	6 years
Initial target dry density			
Upper part $\rho_{d,upper}$ (kg/m^3)	882	882	882
Lower part $\rho_{d,lower}$ (kg/m^3)	1561	1561	1561
Final average dry density			
Upper part $\rho_{d,upper}$ (kg/m^3)	1067	1066	1070
Lower part $\rho_{d,lower}$ (kg/m^3)	1472	1438	1414
Average ρ_d (kg/m^3)	1270	1252	1243

The swelling pressure is measured in four of the ten devices, FLR1-FLR4. The evolution of swelling pressure during the first six years, measured in the device similar to the one used for FLR5-FLR10, is shown in Figure 4-4 where the time for the dismantling of FLR5-FLR7 are marked. Stresses at the time of dismantling of FLR5, FLR6 and FLR7 i.e. after 2, 4 and 6 years are tabulated in Table 4-2. The swelling pressure is given as a total pressure with the applied water pressure included.

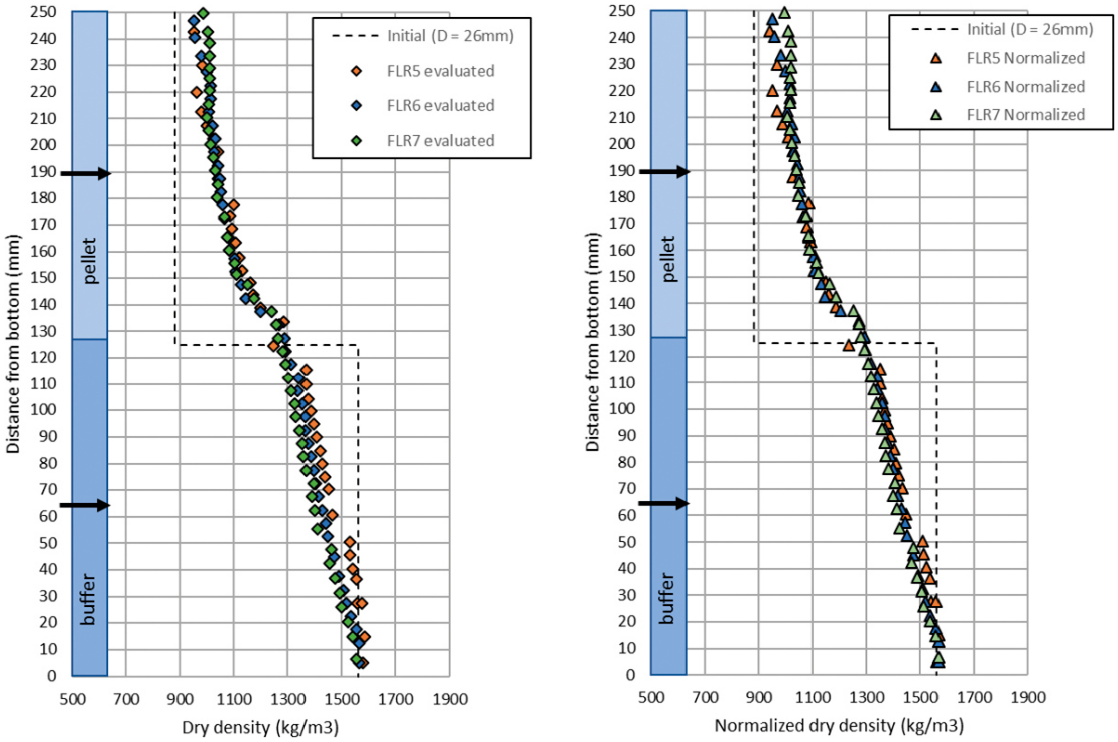

Figure 4-3. *Distribution of measured dry density (to the left) and normalized dry density (to the right) where the dry density is normalized with the ratio of the actual average density to the average dry density of all three specimens (1 255 kg/m^3).*

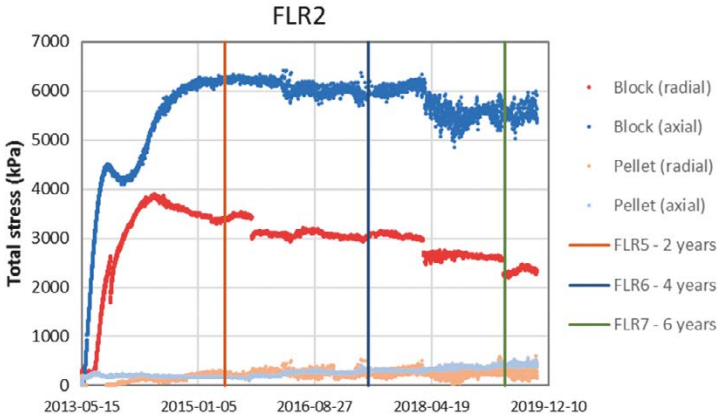

Figure 4-4. *Evolution of swelling pressure as total stress from the start to 2019-10-22 with the time for the dismantling of FLR5, FLR6 and FLR7 marked. The stresses were not measured on the dismantled set-up but on the equivalent set-up of FLR2.*

Table 4-2. Swelling pressure (total stress), from set-up FLR2 with similar set-up as FLR5, FLR6 and FLR7 at the time corresponding to the dismantling of these, i.e. 2, 4 and 6 years, respectively. The distance from the bottom is given.

Type	Distance mm	Swelling pressure 2 years (FLR5) kPa	Swelling pressure 4 years (FLR6) kPa	Swelling pressure 6 years (FLR7) kPa	Direction	Label
pellet	250	179	309	408	axial	FLR2 pellet (axial)
pellet	187.5	247	232	242	radial	FLR2 pellet (radial)
block	62.5	3381	3066	2235	radial	FLR2 block (radial)
block	0	6231	5981	5440	axial	FLR2 block (axial)

4.5 Analysis – Analytical solution

The distribution of bentonite along the tube can be analyzed by use of an analytical model previously used and presented in the report by Dueck et al. (2019). In this model, based on force equilibrium after pore pressure equilibrium, the swelling pressure and the friction between the bentonite and the test device are related according to Equations 4-1 and 4-2 where σ is the stress at the vertical distance z from the bottom, σ_0 is the stress at the distance $z = 0$, r is the radius of the tube and φ is the friction angle between the bentonite and the tube wall (see also e.g. Åkesson et al. 2010). If not measured the swelling pressure σ is proposed to be calculated from Equation 4-3, according to Börgesson et al. (1995), where the references σ_r and e_r have the values $\sigma_r = 1\,000$ kPa and $e_r = 1.1$. The constant β should be $\beta = -0.19$ at these conditions but at densities lower than 1 200 kg/m^3 $\beta = -0.23$ has been used which was found to better fit with test results at these low densities, see test results presented by e.g. Börgesson et al. (1995).

$$\sigma = \sigma_0 \cdot e^{-\frac{2 \cdot z \cdot tan\phi}{r}} \tag{4-1}$$

$$tan\phi = \frac{r}{2 \cdot z} \cdot \ln\left(\frac{\sigma_0}{\sigma}\right) \tag{4-2}$$

$$\sigma = \sigma_r \cdot \left(\frac{e}{e_r}\right)^{1/\beta} \tag{4-3}$$

The swelling pressure is assumed to decrease from its maximum value to the minimum over the so-called transition length L. The total height of the device was designed to include a transition length estimated to be ten times the diameter of the device. With this set-up the initial dry densities of the block and the pellet should prevail at each end, respectively, with a corresponding swelling pressure at saturation. The density distributions determined at dismantling after 2, 4 and 6 years are shown, separately, in Figure 4-5 with manually interpreted transition lengths marked, i.e. 193 mm,

218 mm and 235 mm, respectively. In Figure 4-6 the dry densities at each end are shown as a function of time. The dry density at the end of the block side corresponds to the initial dry density including the radial volume and the value has been more or less constant over the actual time. At the pellet side the dry density is higher than the initial dry density including the radial volume and shown with the dotted lines in Figure 4-5. In the evaluation of transition length, the initial dry density used has therefore been slightly higher than the value shown by the dotted line. The dry density of the upper part of the pellet is increasing with time, Figure 4-6.

The average friction angle (wall friction) can be estimated according to Equation 4-2. The evaluation can be directly based on swelling pressure measurements or it can be based on the density distribution together with a model of the swelling pressure. Figure 4-7 shows friction angles, interpreted in different ways, presented as a function of time.

In Figure 4-7 to the left the friction angles were determined from the measured radial stresses (black diamond), from the radial stresses minus the water pressure applied (black circles), from the density distribution over the same length as the stress measurements (grey triangles) and from the density distribution over the actual transition length (grey square). The swelling pressure was evaluated by Equation 4-3, based on the normalized dry density distribution. The trends of the results to the left in Figure 4-7 are similar.

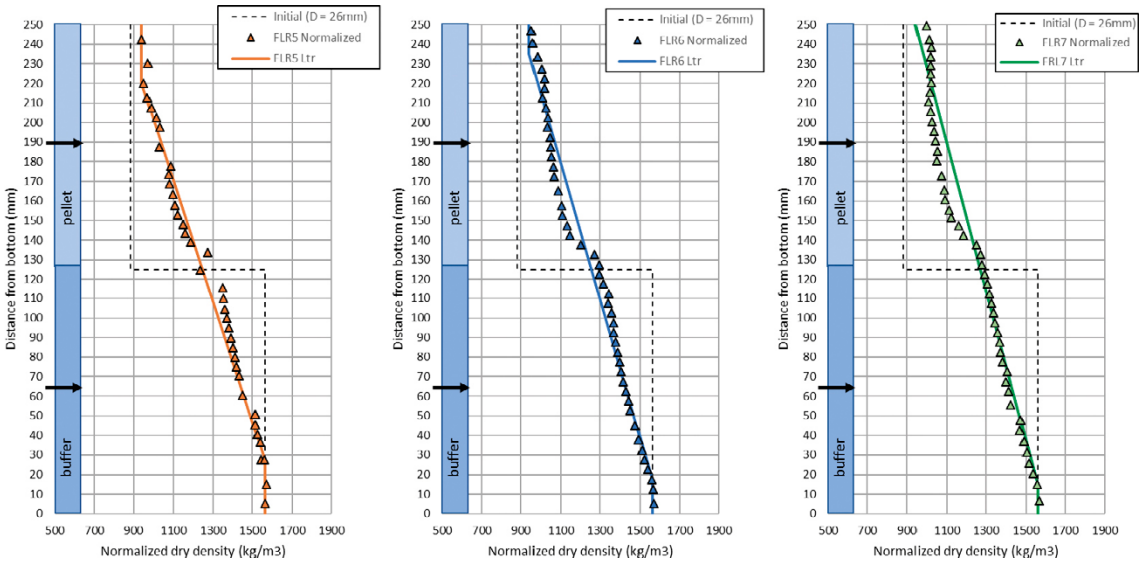

Figure 4-5. *Density distribution at dismantling after 2, 4, and 6 years. The manually drawn lines represent the density distributions over the transition lengths, interpreted as 193 mm, 218 mm and 235 mm, respectively. The initial distributions (dotted lines) are also shown.*

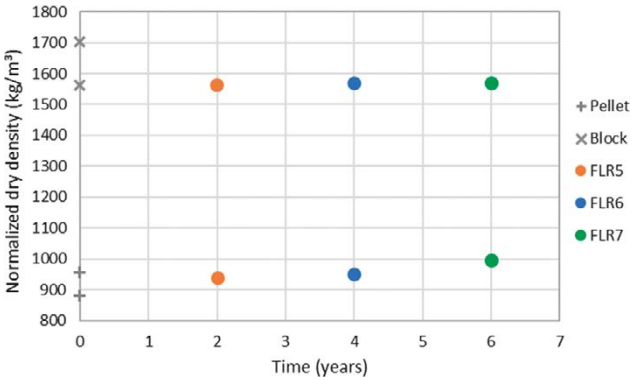

Figure 4-6. *Densities at the upper end (pellet) and lower end (block) as a function of time. The initial dry densities of the pellet and block are marked twice each; corresponding to the installed condition (upper values) and the condition after filling the gaps and grooves after swelling (lower values).*

The friction angles and transition lengths can be evaluated over shorter parts of the bentonite, i.e. over the pellets and the blocks separately. To the right in Figure 4-7 the friction angles evaluated over the pellets (label: pellet ρ) and over the blocks (label: block ρ) are shown. The evaluations were based on transition lengths and density gradients shown in Figure 4-8.

While the friction angle of the pellets decreases with time the friction angle of the blocks is more stable with time. The friction angle of the pellets is the lowest of the evaluated values and the decrease with time is caused by the increasing density at the upper end of the pellet, Figure 4-6. In Figure 4-9 the transition lengths shown in Figure 4-5 and Figure 4-8 are plotted as a function of time.

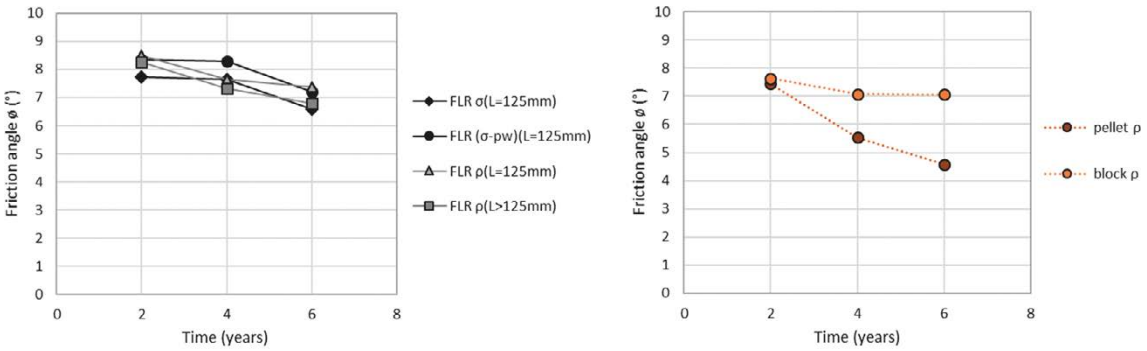

Figure 4-7. *Evaluated friction angles based on measured radial stresses (indicated by σ in the label) or measured density distribution (indicated by ρ in the label) after 2, 4 and 6 years. The results shown to the left are based on parts including both pellets and blocks and to the right the pellets and blocks are evaluated separately.*

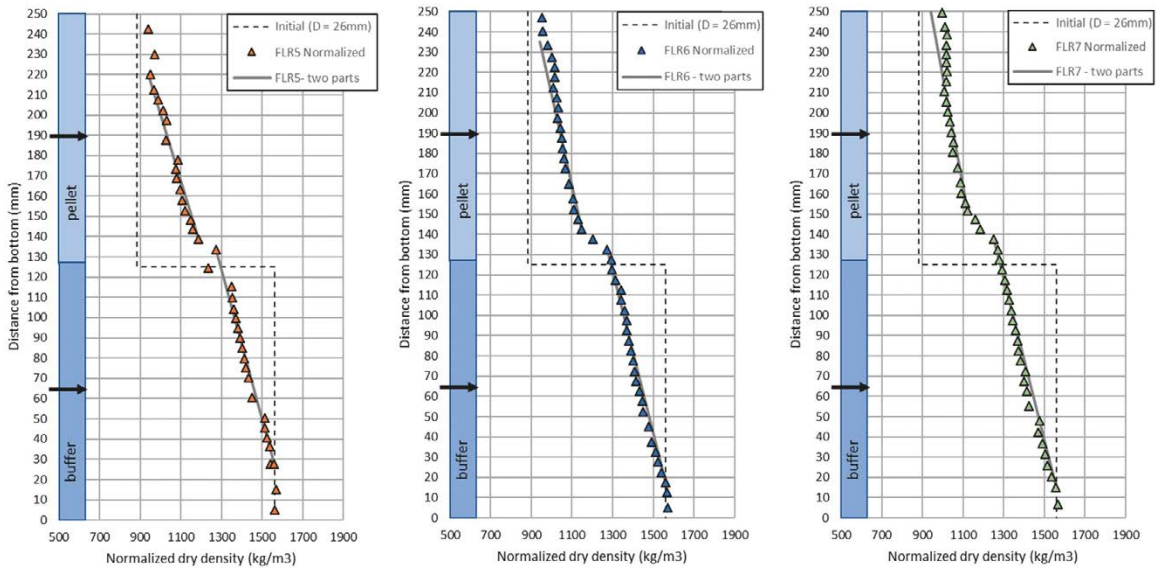

Figure 4-8. *Density distributions at dismantling after 2, 4 and 6 years, from Figure 4-5. The manually drawn lines represent the density distributions over transition lengths evaluated over the pellets and blocks separately.*

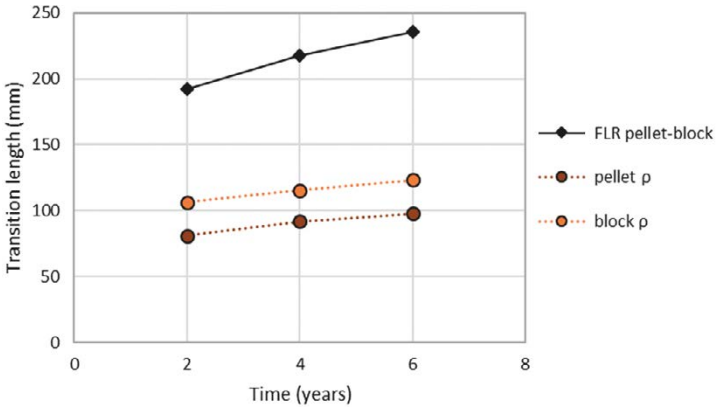

Figure 4-9. *Manually evaluated transition lengths from Figure 4-5 and Figure 4-8.*

The friction angle based on radially measured stresses on the set-up FLR2 was evaluated after 2, 4 and 6 years and shown in Figure 4-7 (label: FLR σ). A continuous evaluation of the friction angle from the radially measured stresses in FLR2 is shown in Figure 4-10. There is a fluctuation in the measured stresses and thereby also in the evaluated friction angle. The fluctuation is mainly caused by variations in temperature also shown in Figure 4-10. However, there seems to be a small decrease in the evaluated friction angle with time which was also seen in Figure 4-7. In the same plot, results from the set-up with a smooth inner wall are also shown (FLR3). The only difference between the set-up used in FLR2 and FLR3 is the surface of the inner wall. The friction angle evaluated from the set-up with smooth inner wall is lower and more constant over time.

The wall friction, evaluated as a friction angle, agrees approximately with residual values determined with friction tests (see e.g. Dueck et al. 2016, 2019). In these tests confined saturated bentonite blocks were forced along a confining ring with the required force measured. From the measured force and the geometry, the wall friction was evaluated as a friction angle. The residual friction angles (evaluated after some displacement) was interpreted to be between 4° and 7° in the actual stress range, see Figure 4-11. This agrees with the friction angles presented above. In the previous study, the influence of the surface of the wall (e.g. plain steel surface, lubricated smooth surface or a surface with grooves) was studied and found to be less than expected. In addition, it was suggested that these residual values were approximately half of the internal friction angle of the bentonite. The internal friction angle is shown with a blue line in Figure 4-11 (Börgesson et al. 1995, Åkesson et al. 2010).

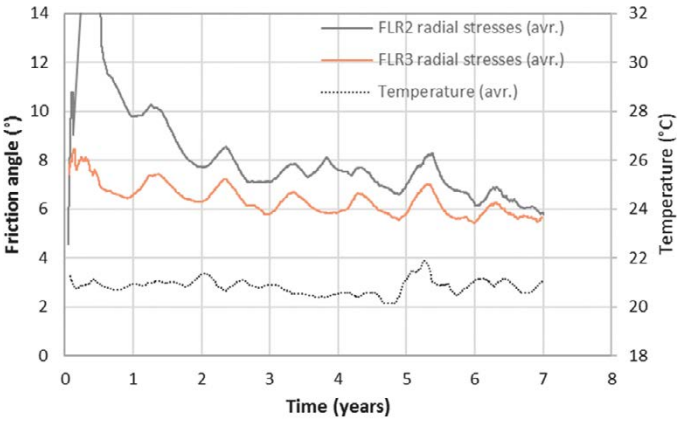

Figure 4-10. *Continuously evaluated friction angle from Equation 4-2 and measured stresses from the set-up analysed above (FLR2) and a set-up with smooth inner wall (FLR3).*

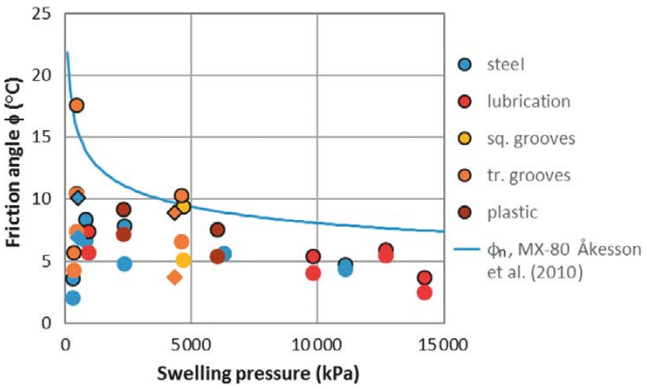

Figure 4-11. *Test results (Dueck et al. 2019) presented as friction angle as a function of swelling pressure. Different types of wall surfaces were used (e.g. plain steel, lubricated wall or wall with grooves). Peak values are plotted with marker lines and residual values without marker lines. The blue line represents the internal friction angle of the bentonite.*

4.6 Concluding remarks

A test series of long-time homogenisation tests in steel tubes are ongoing. By using different test durations before termination together with sampling, the influence of time and creep on the distribution of density can be studied. Three tests have been finished after 2, 4 and 6 years while seven are still ongoing which can give more information about the influence of time on the homogenisation when dismantled.

The analysis shows that the understanding of the homogenisation can be further explained and understood by use of the analytical model used and from the model a reasonable friction angle can be evaluated. A previous analysis presented in the report by Dueck et al. (2019) gave a friction angle $\varphi = 7°$ after two years. The analysis here, based on additional results after four and six years, suggests a slightly lower value after six years. The lower friction angle, approximately 6°, agrees with a friction angle evaluated from a similar set-up but with smooth inner wall and with the residual friction angle evaluated after some displacement in friction tests.

5 Final comments

To increase the knowledge of the homogenisation process an SKB project has been running during several years. Based on tests and results from this project analyses of some specific test results have been made and the results have been presented as the three following analyses:

1) Comparison of homogenisation and sealing behaviour of calcium bentonite and sodium bentonite.
2) Comparison of homogenisation and sealing behaviour of bentonite after rapid and slow water uptake.
3) Comparison of homogenisation of bentonite in long steel tubes after two, four and six years.

Each study has been presented independently, in different chapters, with the intention to be used as basis for poster presentations. Concluding remarks and suggestions for additional work are given in each chapter.

References

SKB's (Svensk Kärnbränslehantering AB) publications can be found at www.skb.com/publications.

Börgesson L, Johannesson L-E, Sandén T, Hernelind J, 1995. Modelling of the physical behaviour of water saturated clay barriers. Laboratory tests, material models and finite element application. SKB TR 95-20, Svensk Kärnbränslehantering AB.

Börgesson L, Åkesson M, Hernelind J, 2020. EBS-TF – THM modelling. Homogenisation task. SKB P-18-05, Svensk Kärnbränslehantering AB.

Dueck A, Goudarzi R, Börgesson L, 2011. Buffer homogenisation, status report. SKB TR-12-02, Svensk Kärnbränslehantering AB.

Dueck A, Goudarzi R, Börgesson L, 2014. Buffer homogenisation, status report 2. SKB TR-14-25, Svensk Kärnbränslehantering AB.

Dueck A, Goudarzi R, Börgesson L, 2016. Buffer homogenisation, status report 3. SKB TR-16-04, Svensk Kärnbränslehantering AB.

Dueck A, Goudarzi R, Börgesson L, 2018. Buffer homogenisation – status report 4. SKB TR-17-04, Svensk Kärnbränslehantering AB.

Dueck A, Goudarzi R, Jensen V, Börgesson L, 2022. Buffer homogenisation – status report 5. SKB TR-21-14, Svensk Kärnbränslehantering AB.

Dueck A, Börgesson L, Kristensson O, Malmberg D, Åkesson M, Hernelind J, 2019. Bentonite homogenisation. Laboratory study, model development and modelling of homogenisation processes. SKB TR-19-11, Svensk Kärnbränslehantering AB.

Karnland O, Olsson S, Nilsson U, 2006. Mineralogy and sealing properties of various bentonites and smectite-rich clay materials. SKB TR-06-30, Svensk Kärnbränslehantering AB.

Svensson D, Dueck A, Nilsson U, Olsson S, Sandén T, Lydmark S, Jägerwall S, Pedersen K, Hansen S, 2011. Alternative buffer material. Status of the ongoing laboratory investigation of reference materials and test package 1. SKB TR-11-06, Svensk Kärnbränslehantering AB.

Åkesson M, Börgesson L, Kristensson O, 2010. SR-site Data report, THM modelling of buffer, backfill and other system components. SKB TR-10-44, Svensk Kärnbränslehantering AB.

Arkitektkopia AB, Bromma, 2022

SKB is responsible for managing spent nuclear fuel and radioactive waste produced by the Swedish nuclear power plants such that man and the environment are protected in the near and distant future.

skb.se